ACS Catalysis

RESEARCH ARTICLE

pubs.acs.org/acscatalysis

Solvent Evaporation Assisted Preparation of Oriented Nanocrystalline Mesoporous MFI Zeolites

Kake Zhu,[†] Junming Sun, Jun Liu,* Liqiong Wang, Haiying Wan, Jianzhi Hu, Yong Wang, Charles H. F. Peden, and Zimin Nie

Pacific Northwest National Laboratory, Richland, Washington 99352, United States

ABSTRACT: A solvent evaporation route to produce hierarchically porous zeolites with an oriented MFI nanocrystalline structure has been developed, and the method is scalable and low cost. In this method, hexadecyltrimethoxysilane is added to an ethanol solution containing zeolitic precursors. A dry gel is formed during the evaporation process. Subsequent hydrothermal treatments produce the hierarchically porous zeolite. High resolution transmission electron microscopy (HRTEM) studies suggest that misoriented zeolite nuclei are produced in the early stages of the hydrothermal treatment, but further reactions lead to single crystal-like aggregates composed of intergrowth nanocrystals with a mean interparticle pore diameter of 12 nm. Almost all Al atoms exist in tetrahedral sites, as confirmed by ^{27}Al magic angle spinning nuclear magnetic resonance (MAS NMR). Variable temperature hyperpolarized (HP) ^{129}Xe NMR spectroscopy suggests a fast molecular diffusion process from the interconnection between micro- and mesopores. Catalytic conversion of acetone to isobutene reactions shows comparable (with respect to conventional zeolites) selectivity to isobutene. However, hierarchically porous zeolites display enhanced activity and durability because of the more accessible acidic sites in the hierarchically porous structures.

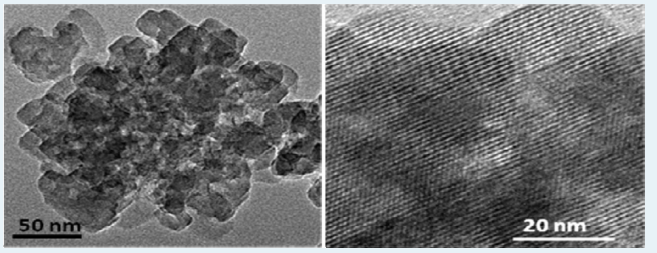

KEYWORDS: ZSM-5, zeolites, hierarchical structure, mesoporous, catalyst, acetone, isobutene

INTRODUCTION

Zeolites are crystalline microporous (<2 nm, typically 0.4 to 1.2 nm in size) solids with channels and cages comparable to molecular sizes. Their pore walls are constructed of tetrahedral metal oxide units that consist primarily of Si, Al, P, or sometimes transition metals. When an Al^{3+} substitutes a Si^{4+} site in the zeolite framework, an ion exchangeable +1 cationic site is created to maintain the charge balance.[1] These sites in the internal micropores of zeolites are locations for redox and acid−base chemical reactions, depending on the nature of the charge-balancing cations. In addition, confinement effects in these channels are capable of tailoring reaction pathways to desirable products by shape selectivity via reactants, intermediates, or transition states. Zeolites display considerable hydrothermal stability even under harsh reaction conditions because of their crystallinity. These intrinsic properties make zeolites broadly applicable in heterogeneous catalysis for petroleum refining to produce fuels and chemicals, as adsorbents for separation processes, and in the laundry industry as ion-exchangers.[2] On the other hand, the built-in micropores and micrometer-sized crystallites of zeolites impose diffusion limitations for these applications as a result of the overall length of the pores.[3] Circumventing such diffusion limitations will facilitate mass transfer inside the microporous system, thereby enhancing the activity and efficiency of zeolite-based catalysts.

Several strategies have been employed to improve accessibility to micropores inside zeolites: making wide pore zeolites, decreasing the crystal sizes of zeolites to nanometer scale dimensions, and creating additional porosity to conventional zeolites.[3−5] Among them, nanozeolite (NZ) and hierarchically porous zeolite (HPZ) syntheses have attracted much attention for their stability and generality as preparation methods and their practicality in scaled-up and improved catalytic performances.[3] Approaches for NZ and HPZ syntheses can be divided into controlled zeolite crystallization, templating methods, and postsynthetic treatments. The size of zeolites is normally reduced to nanometer dimensions by confinement using carbon blacks or thermally reversible polymer hydrogels,[6,7] inhibitors to stop the growth of zeolitic seeds,[8−13] or microemulsions.[14] The additives used provide a steric hindrance that confines crystallization to produce discrete NZs. Most of these methods use a dilute solution with a low yield; therefore, such syntheses can be difficult to scale up for industrial level applications. Moreover, in the molecular inhibitor assisted approach, it is necessary to adopt preformed zeolitic seeds for the growth, which adds processing complexity and makes the method expensive and labor intensive. HPZ synthesis using carbon black as a hard template during zeolite crystallization was first described by Jacobsen and co-workers where subsequent combustion removal of carbons creates additional porosity in these crystals.[15−18] The zeolites they prepared

Special Issue: Victor S. Y. Lin Memorial Issue

Received: February 17, 2011
Revised: March 30, 2011
Published: May 19, 2011

possess additional mesopores to zeolitic micropores and have shown improved activity in acid catalyzed and redox reactions, or as catalyst supports.[15−18] This result has initiated significant effort to explore other routes for HPZ preparation. Hard templates, such as cationic polymers, mesoporous carbon, or carbon hydrates, are being investigated to create additional porosity.[19−23] In addition, Ryoo's group has designed a supermolecular (soft-templating) approach to prepare HPZs with an organosilane $[(CH_3O)\text{-}SiC_3H_6N(CH_3)_2C_nH_{2n+1}]^+Cl^-$ as both the silicon source and structure directing agent.[24] The HPZ material is ordered in both crystallinity and mesophase, as evidenced by the small and wide-angle X-ray diffraction (XRD) patterns. The porosity could also be tuned through a chain length of hydrophobic tails. MFI-structured HPZ has also been prepared using silylated polyethylenimine polymers both as the template for additional porosity and as the siliceous source; as a result, quite small (<10 nm) mesopores are created.[25] Still, the surfactants used for these materials are not commercially available and are expensive, as pointed out in a recent review by Christensen et al.[4] Alternative methods are desirable to synthesize nanocrystalline and hierarchical porous zeolites with tunable porosity NZs that reduce cost and are readily scalable.

In this paper, we report a facile method to prepare HPZ with MFI-structured ZSM-5 using a solvent evaporation hydrothermal reaction method. Commercial hexadecyltrimethoxysilane (HTS) and tetrapropylammonium hydroxide (TPAOH) are used as structure-directing agents. An evaporation-induced assembly is an effective way to produce mesoporous materials with ordered mesophase.[26−28] In the past, organoalkoxysilanes have been found to undergo evaporation-induced self-assembly and form mesophases with mostly lamellar and occasionally hexagonal structures. However, only amorphous pore walls are produced.[29−32] A combination of solvent evaporation induced self-assembly with hydrothermal zeolite growth will pave new ways to control crystallization and will provide new methods to tailor hybrid materials. This approach can be scaled up to meet commercial processing, and can be adapted for recyclable solvents.[33,34]

We used an ethanol solution of HTS, tetraethylorthosilicate (TEOS), and TPAOH as the starting solution to form a hard gel to lock in all reactants during evaporation, which is transformed into zeolite nanocrystalline structures in the hydrothermal treatment. In our study, ethanol was chosen for the following reasons: (1) ethanol is a compatible medium for both organophilic ingredients (HTS, TEOS, and aluminum tritert butoxide [ATTB]) and hydrophilic TPAOH aqueous solution, (2) ethanol is a product after TEOS hydrolysis and slows down the hydrolysis of TEOS, (3) ethanol is an ideal solvent for most solvent evaporation-induced self-assembly processes,[41] and (4) ethanol is cheap and environmentally benign. The zeolites prepared in this way possess aggregates of primary zeolitic particles between 10 and 50 nm, and in each aggregate the primary zeolite crystals share the same crystalline orientation to form a single crystal-like HPZ. XRD, TEM/HRTEM, ^{27}Al MAS NMR, and nitrogen sorption results demonstrate that the obtained material has hierarchical porosity. Variable temperature HP ^{129}Xe NMR spectra suggest a fast molecular diffusion process from the interconnection between micro- and mesopores. A probe reaction from acetone to isobutene further confirms that the mesoporous zeolites indeed facilitate the mass transfer of guest species and possess more accessible acidic sites, resulting in its higher activity and durability.

EXPERIMENTAL SECTION

Chemicals. TEOS (99%) and TPAOH (40% w/w aqueous solution) were obtained from Fluka and Alfa Aesar, respectively. Ethanol (90%), ATTB (99%), and ammonium hydroxide (28 to 30%) solutions were purchased from Aldrich, while HTS was obtained from Gelest. All chemicals were used directly without further purification. DI-H_2O is house made using a Barnstead Easypure RODI system. Operations before hydrothermal treatment were conducted under ambient conditions.

Synthesis. Hydrothermal treatment of the dry gel produces HPZ, labeled here as ZSM-5-HTS. ZSM-5-HTS has both additional porosity and shortened diffusion pathways for molecules adsorbed inside its micropores, while its single-crystal nature makes it easier to handle compared with NZ. In a typical synthesis of ZSM-5-HTS, 3.12 g of TEOS, 0.21 g of HTS, and 0.07 g of ATTB were dissolved in 10.0 mL of ethanol under stirring. This mixture was further stirred for 30 min to form a solution, followed by adding another solution of 2.0 g of TPAOH in 2.0 g of ethanol under vigorous stirring. Hydrolysis occurred at this stage, as suggested by the appreciable heat release, and a "clear solution" was produced that is stable for more than one month. The clear solution was stirred for 1 h before being transferred to a Petri dish where the solvent was allowed to evaporate overnight. A transparent dry gel was produced during solvent evaporation, which was placed in a Teflon cup. The cup was placed in a Teflon-lined autoclave of 123 mL, and 5.0 g of water was added outside the cup to create steam for the hydrothermal synthesis conditions. The autoclave was placed in an oven set at 177 °C and kept for up to 5 days for a moisture-assisted hydrothermal crystallization. The final solid, retaining the shape of the original dry gel, was filtrated and washed with water and then calcined at 550 °C for 20 h by a ramp of 3 °C/min in air. To prepare a conventional ZSM-5 with the same Si/Al ratio, 3.24 g of TEOS, 0.07 g of ATTB, 2.0 g of TPAOH, and 7.7 mL of ammonium hydroxide were mixed in 30.0 g of DI-H_2O and stirred for 4 h. The solution was then transferred to an autoclave and allowed to crystallize for 72 h at 177 °C.[35] The template was removed by combustion with the same procedure as for ZSM-5-HTS. For both samples, the Si/Al molar ratio was 70 determined by elemental analysis.

Characterizations. The XRD patterns in the θ-2θ scan mode were obtained on a Philips Xpert X-ray diffractometer using Cu Kα radiation at λ = 1.54 Å. Nitrogen sorption data were collected with a Quantachrome autosorb-6 automated gas sorption system. Before physisorption measurements, all samples were outgassed under vacuum at 180 °C overnight. The total surface areas were determined by the Brunauer−Emmett−Teller (BET) method, and micropore volumes were calculated by the *t*-plot method. Total pore volumes were estimated from the amount of N_2 adsorbed at p/p_0 = 0.99. Meso-/macro- pore volumes were calculated by subtracting micropore volumes from total pore volumes. The Barret−Joyner−Halenda (BJH) calculation was employed to estimate the pore-size-distribution for the mesoporous samples. Scanning electronic microscopy (SEM) was conducted on a JEOL JSM-5900LV at 20 kV. Transmission Electron Microscope (TEM) studies were conducted on a JEOL JEM 2010 microscope operated at 200 kV. Thermogravimetric (TG) analysis was conducted on a NETZSCH, STA 409 CD. The flow rates for sample and reference were both 10 mL/min, and the ramping temperature was 10 °C/min, from 35 to 1000 °C. The mass for both samples was about 7.0 mg.

A Varian chemagnetics spectrometer (7.05 T, 300 MHz) equipped with a variable temperature double-resonance probe

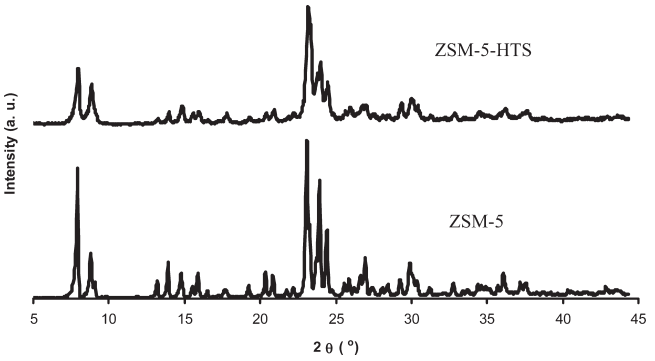

Figure 1. XRD patterns of ZSM-5 and ZSM-5-HTS powders after template removal.

was used for ^{27}Al Magic Angle Spinning (MAS) Nuclear Magnetic Resonance (NMR). Samples were loaded into 5-mm zirconia PENCILTM rotors and spun at 5 to 10 kHz. Spectra of ^{27}Al MAS NMR were collected at 78.2 MHz with a 0.5 μs ^{27}Al pulse and a repetition delay of 1 s. We used a 40-ms acquisition time, a 50-kHz spectral window, and a 24-Hz Lorentzian line broadening. Chemical shifts of ^{27}Al NMR were referenced to 0.1 M $Al(NO_3)_3$ at 0 ppm.

HP ^{129}Xe NMR experiments were carried out on a Varian chemagnetics spectrometer operating at 82.98 MHz (magnetic field 7.05 T) with a homemade variable-temperature double-resonance MAS probe under a continuous flow (CF) of HP xenon. For ^{129}Xe NMR experiments, a single-pulse (SP) Bloch-decay method was used, and samples were loaded into 7.5-mm Zirconia PENCIL rotors. SP spectra were collected with a 4.5-μs (90°) ^{129}Xe pulse and a repetition delay of 1 s. The number of transients was 100. The HP Xe gas was produced with a home-made HP ^{129}Xe polarizer described previously.[36]

Catalysis. The acetone to isobutene reaction was conducted in a fixed-bed stainless steel reactor (i.d., 5 mm). Typically, a 0.1 g sample was mixed with 0.9 g of SiC dilutes and then packed between quartz wool beds. The thermocouple was placed at the middle part of the catalysts bed for temperature monitoring. Before the reaction, samples were activated at 350 °C (5 °C/min) under N_2 flow (42 STP mL/min) for 30 min, after which the temperature was lowered to 330 °C for the catalytic test. After holding for 10 min at 330 °C, acetone was pumped into the evaporator (180 °C). The evaporated acetone gas was then carried into the reactor by the flowing nitrogen gas (25 STP mL/min, $P_{acetone}$ = 4.0 mol %). The reactor tubes downstream were heated to more than 150 °C to avoid the condensation of any products before analysis. The effluent gas was sampled by an autosampling valve (170 °C) and analyzed by an online gas chromatograph (GC) (Shimadzu 2400) equipped with a Flame Ionization Detector (FID). The column was an HP-Plot Q micro capillary column (30 m, 0.53 mm, 40 μm). After a cold trap, the unreacted acetone and liquid products were condensed, and dry gas was sent to a micro-GC (Micro3000A equipped with molecular sieves 5A, plot U columns, and Thermal Conductivity Detectors [TCD]) for analysis. N_2 was used as reference gas.

RESULTS AND DISCUSSIONS

An XRD pattern of the as-synthesized HPZ is shown in Figure 1, together with an XRD of conventional MFI-structured ZSM-5 for comparison. These patterns coincide with reported MFI-structured

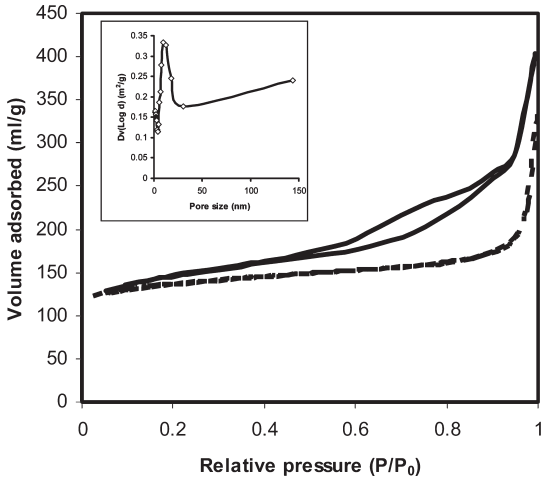

Figure 2. Nitrogen adsorption−desorption isotherms of conventional ZSM-5 (dashed line) and ZSM-5-HTS (solid line). A pore-size distribution deduced from the adsorption branch of the isotherm for ZSM-5-HTS is shown in the inset.

Table 1. Nitrogen Physisorption Analyses of ZSM-5 and ZSM-5-HTS

sample	S_{BET}, m^2/g	micropore, vol. (mL/g)[a]	meso + macro, vol. (mL/g)[b]	mesopore, dia. (nm)
ZSM-5	408	0.16		
ZSM-5-HTS	451	0.14	0.49	~12

[a] Micropore volume is estimated using the *t*-plot method. [b] Mesopore + macropore volume is calculated by a subtraction of total pore volume at a relative pressure of P/P_0 = 0.99 from the micropore pore volume obtained from the *t*-plot method.

materials of the same type (JCPDS 00-043-0784), and no additional crystalline phase or amorphous silica was observed.[37] ZSM-5-HTS shows some broadening of the diffraction peaks and relatively weak intensity as compared to the conventionally prepared ZSM-5 catalyst, similar to observations also reported in NZ or HPZ syntheses.[8,17,19,22] This result demonstrated a decrease in crystalline size of the primary zeolitic particles.

The N_2 physisorption isotherms of conventional ZSM-5 and ZSM-5-HTS are given in Figure 2. The high starting point of nitrogen adsorption at P/P_0 of 0.03 shows that micropores of ZSM-5 and ZSM-5-HTS were filled at even low pressures. By a *t*-plot method estimation, micropore volumes of 0.16 and 0.14 mL/g can be attributed to ZSM-5 and ZSM-5-HTS, respectively. For conventional ZSM-5, no obvious uptake of nitrogen can be identified in the relative pressure range from 0.03 to 0.95, indicating that there were no mesopores (Table 1). For ZSM-5-HTS, the uptake of nitrogen increased linearly with pressure between 0.03 and 0.7, and a jump of nitrogen uptake was observed above 0.7. The curve is categorized as a type IV isotherm, a typical pattern for mesoporous materials. A hysteresis loop above 0.45 was also observed, but this could be a "real" type-H1 hysteresis loop, or it could be from the so-called "tensile strength effect" (TSE).[38] To exclude such an ambiguity, it is better to calculate pore-size distributions from the adsorption than the desorption branch. Through the BJH method, a pore-size distribution was obtained as shown in the Figure 2 inset, clearly showing a broad pore size between 5 and 30 nm centered

dx.doi.org/10.1021/cs200085e |*ACS Catal.* 2011, 1, 682–690

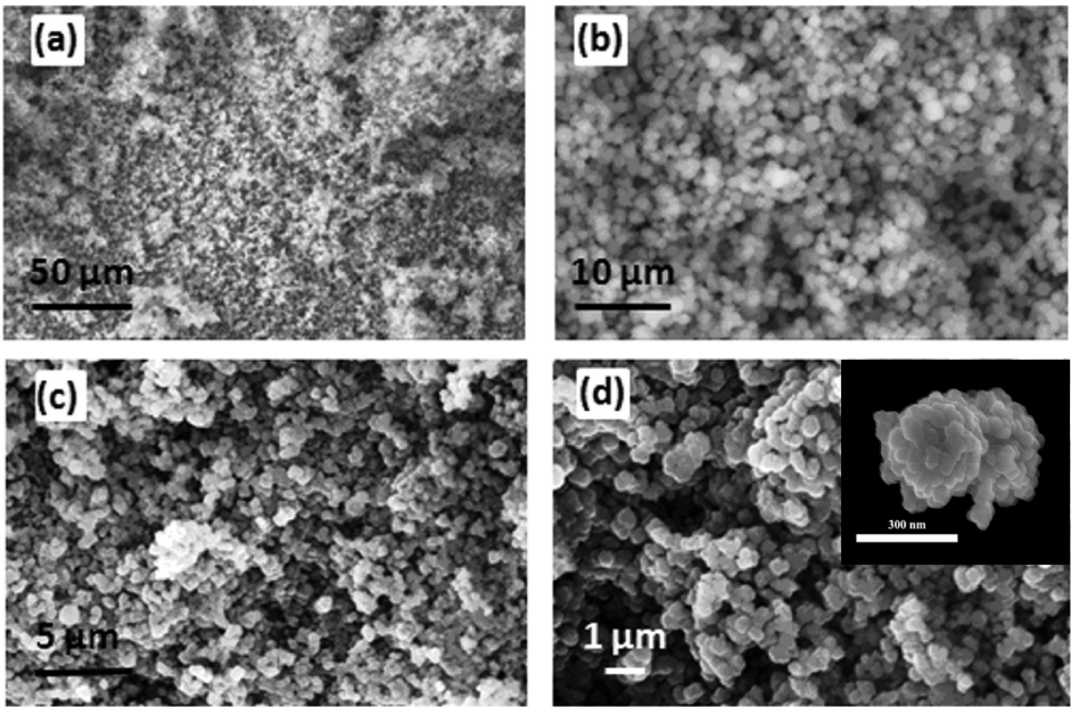

Figure 3. SEM micrographs of ZSM-5-HTS after combustion removal of the organic structure directing agents, at low (a, b) and high (c, d) magnifications. Inset in Figure 3d clearly shows one single secondary particle aggregate with primary nanozeolites.

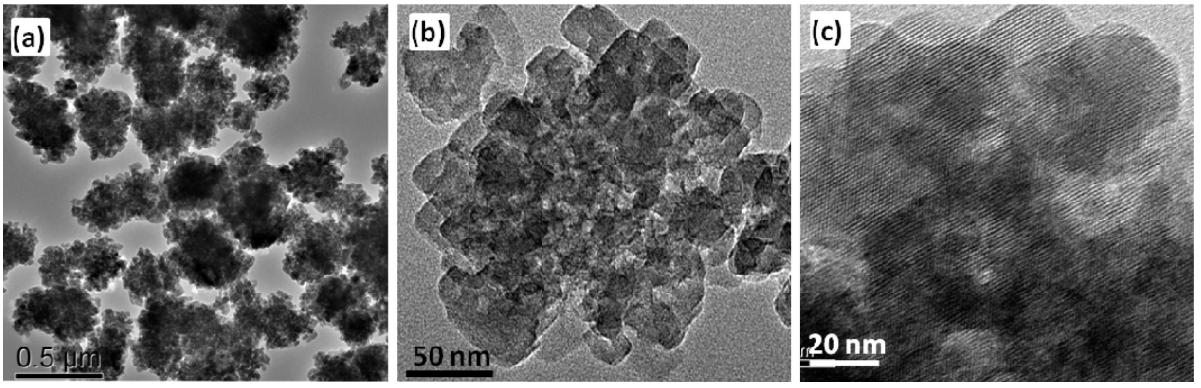

Figure 4. TEM images of ZSM-5-HTS: low-magnification images (a) and (b) show that aggregates of powder are composed of nanoscale zeolitic particles. A higher resolution micrograph (c) reveals that particles share the same crystalline orientation.

at 12 nm. Besides a micropore volume of 0.14 mL/g, an additional pore volume of 0.49 mL/g for ZSM-5-HTS is attributed to macro- and mesopore volumes (Table 1). This is different from conventionally prepared ZSM-5.

Figure 3 displays SEM micrographs of ZSM-5-HTS to elucidate the microscopic structure of the material. From Figures 3a and 3b, low-magnification SEM images demonstrate the homogeneity of the sample. The powder was made up of uniformly semispherical particles of diameters between 1 and 2 μm. During hydrothermal crystallization, the precursors merged to form zeolites accompanied by substantial morphological changes. When we zoomed in to observe the morphology, these small spheres were sponge-like on their surfaces (Figure 3c and 3d), suggesting that there may be additional pores inside each sphere. Normally under SEM, conventional zeolites have quite clear edges and corners because of their well-defined morphologies, while hierarchically structured or porous zeolites are sponge-like.[16,21] The typical coffin-like shape of MFI-structured zeolite observed in HPZ prepared with the hard template method cannot be found in these images.[14,15] HPZ from the soft template method is different in shape from those prepared with the hard template, a phenomenon found also in Ryoo's work.[20] This is because the formation mechanisms are different. In the hard template route, the chemically inert template (such as carbon or polymer) is embedded in zeolitic crystals during their growth. The energetically favorable shapes of parent zeolites can be maintained. In the soft-template synthesis that we used here, the HTS played a role as both the siliceous source and the growth inhibitor. The hydrocarbon chains on the particle surface inhibited the crystal growth and limited the crystal sizes.

To explore the basic building blocks for ZSM-5-HTS in more detail, TEM was used, and images are displayed in Figure 4. In

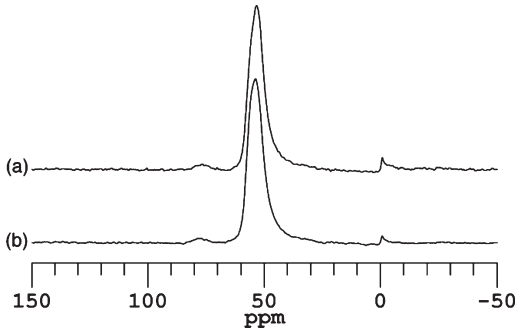

Figure 5. Solid-state ^{27}Al MAS NMR spectra taken at 25 °C for (a) ZSM-5 and (b) ZSM-5-HTS using an MAS spinning rate of 2 kHz.

low-magnification images (Figure 4a), 200 to 500 nm aggregates are seen for the entire sample, indicating that the powder consisted of secondary aggregates that correspond to the 1 to ~2 μm spheres observed in the SEM measurements. A high-magnification TEM image (Figure 4b) suggests that the aggregates were made of rectangular nanoparticles ranging from 10 to 50 nm. These rectangular nanoparticles seem to be aligned in the same direction. In addition, voids were created within crystallites and aggregates to form additional mesoscale porosity. The interparticulate mesopore does not have well-defined shape and orientation. This structure is quite similar to the first HPZ reported by Jacobsen and co-workers, except that the overall size of each single crystal is much smaller than theirs, ~0.3 to 1.2 μm.[15] HRTEM (Figure 4c) further reveals that the nanoparticles were crystalline in nature. Surprisingly, the lattice fringes from all the nanoparticles in the same aggregate were in the same direction, indicating that all the nanoparticles were crystallographically aligned like a single crystal. The lattice fringes in the high resolution images are about 0.96 nm and correspond to the (111) planes of the crystals. The mesoporosity cannot be easily observed in the high resolution TEM image because the crystals are aligned and the morphological contrast is minimized in the phase contrast mechanism.

Figure 5 displays solid-state ^{27}Al MAS NMR spectra taken at 25 °C for ZSM-5 and ZSM-5-HTS with the use of MAS spinning rates of 2 kHz. These spectra can be used to determine the local chemical environment around the Al atoms for these two zeolites. For both samples, Figure 5 exhibits a large signal at ~54 ppm and a negligible peak at 0 ppm. On the basis of previous studies,[39] the signal position of 54 ppm is typical for $Al(OSi)_4$ units, representative of tetrahedral-coordinated framework Al with four Al−O−Si bonds. The small peak at 0 ppm can be attributed to the existence of a small amount of extra-framework octahedral Al. Besides, a broad shoulder was also observed at about 80 ppm, which is due to the spinning sideband. Both ZSM-5-HTS and ZSM-5 contain similar tetrahedrally coordinated framework Al species.

Variable-temperature HP ^{129}Xe NMR spectra for ZSM-5 and ZSM-5-HTS are shown in Figure 6. In addition to a free Xe gas peak at 0 ppm, these samples exhibited a large signal at chemical shifts >100 ppm, which shifted to higher chemical shifts with decreasing temperature. The increased quantity of adsorbed Xe on the surface of the zeolites at reduced temperatures resulted in these larger observed chemical shifts. Since there are mostly micropore channels in ZSM-5, the large signal at >100 ppm can be readily attributed to Xe molecules adsorbed in these framework micropore channels. However, it is surprising to observe only one large signal at

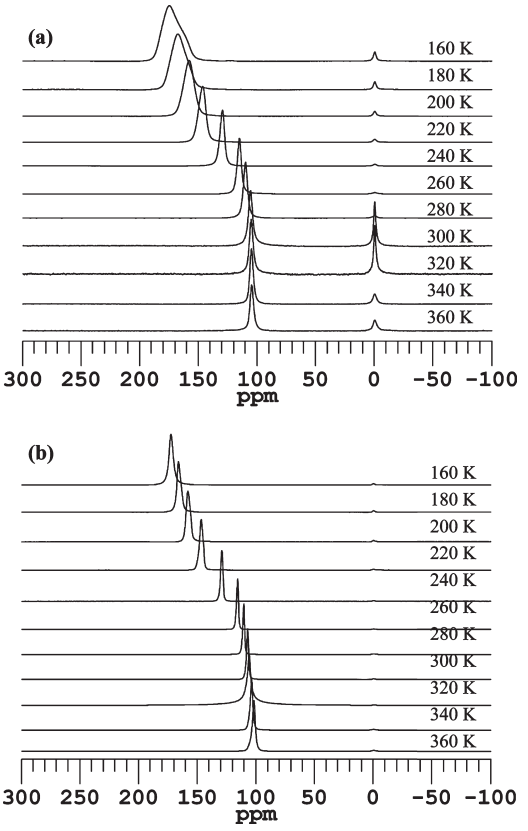

Figure 6. Variable-temperature HP ^{129}Xe NMR spectra for (a) ZSM-5 and (b) ZSM-5-HTS.

>100 ppm for ZSM-5-HTS. In principle, if Xe does not undergo exchange between two different pore regions, two separate signals corresponding to micro- and mesopores will be observed. In fact, a previous study reported two distinct peaks for mechanically mixed mesoporous silica and ZSM-5 where the micro- and mesopores are in different domains.[40] Although all of our results so far suggest the existence of both mesoporous and microporous channels in the ZSM-5-HTS framework, the absence of the two peaks (not including the gas-phase peak) at lower temperatures suggests that the Xe exchange rate between meso- and micropores persists in the fast-exchange regime, even at temperatures as low as 160 K. Highly interconnected channels between micro- and mesopores are most likely the reason for such a rapid exchange of Xe for ZSM-5-HTS. At a given temperature, the Xe exchange rate between different pores largely depends on the degree of the connectivity among different pore channels. The observation of two distinct peaks in the previous mechanical mixture of mesoporous silica and ZSM-5 suggests fewer connected pores between micro- and mesochannels as compared with our ZSM-5-HTS.[40]

Figure 7a displays the temperature dependence of the adsorbed ^{129}Xe chemical shifts for ZSM-5 and ZSM-5-HTS. Temperature-dependent chemical shifts for the samples were similar because both contained the ZSM-5 zeolite framework with the same Si/Al ratio. A similar chemical-shift dependence was also observed in previous studies of mesoporus ZSM-5 zeolites.[40] Although our ZSM-5 and ZSM-5-HTS gave identical temperature-dependent chemical shifts, their temperature-dependent line-widths were very different (Figure 7b). For ZSM-5-HTS, the line-width remained relatively constant over the entire

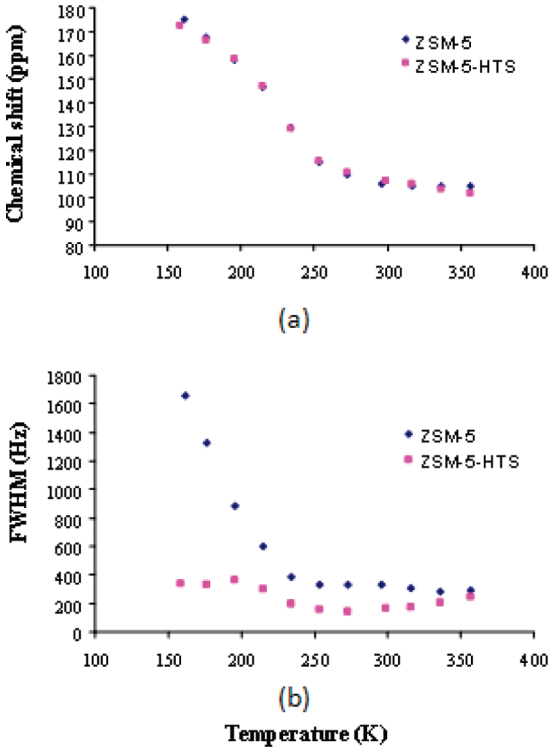

Figure 7. Temperature dependence of adsorbed ^{129}Xe chemical shifts for (a) ZSM-5 and ZSM-5-HTS and (b) their temperature-dependent line-widths.

temperature range from 360 to 160 K, whereas the line-width for ZSM-5 exhibited significant broadening at $T < 240$ K. The ZSM-5 line width increased from 380 Hz at 240 K to 1660 Hz at 160 K while the ZSM-5-HTS maintained a line width of ≈300 Hz throughout the temperature range. The large difference in line width for ZSM-5 and ZSM-5-HTS is in contrast with results obtained in the previous study where both meso ZSM-5 and commercial ZSM-5 gave similar temperature-dependent line widths. For materials having the same crystal structures and chemical compositions, the line width is largely determined by the homogeneity of the pores as well as how fast the Xe exchanges between the different types of pores. Since both ZSM-5 and ZSM-5-HTS have the same micropore structures, and they are both crystalline materials, the difference in line width is mostly determined by how fast that Xe can travel in and out of different pores. The relatively sharp resonance observed even at a low temperature for ZSM-5-HTS suggests that Xe is in rapid exchange with both micro- and mesopores. Such high exchange rates result from the highly connected pores in the unique hierarchical structures of our ZSM-5-HTS. Our ^{129}Xe NMR data suggest that the connectivity between micro and mesochannels in our ZSM-5-HTS was higher than those of meso-ZSM-5 reported in the previous work.[40] Our XRD, BET, and TEM data show that ZSM-5-HTS was composed of very small 10 to 50 nm crystals that were aggregated in the same crystal orientation. The mesopores were mostly from the interparticle spacing, which allows Xe to rapidly exchange from the meso- to microchannels, resulting in a single sharp ^{129}Xe NMR peak. The decrease in zeolite size observed in TEM measurements and the mesoporosity formed from the voids between crystallites and aggregates provides the unique hierarchical structures of ZSM-5-HTS as compared with the meso ZSM-5 synthesized in a previous study.[40] Such unique structures lead to the high connectivity between meso- and micropores, consistent with our ^{129}Xe NMR findings. The high connectivity of the different-scale pores would facilitate mass transfer, and provide more accessible acidic sites in the zeolites. As a result, a higher catalytic activity was observed on ZSM-5-HST compared with the traditional ZSM-5, which will be discussed in the following part.

As far as the NZ or HPZ formation mechanism is concerned, HTS, TEOS, and ATTB first dissolve in ethanol to form a homogeneous solution. After adding the TPAOH ethanol mixture, HTS, TEOS, and ATTB start to hydrolyze to form a sol. This hydrolysis is accompanied by a heat release since the reaction is exothermic. As hydrolysis proceeds, small hydrophilic moieties, such as AlO_x-, SiO_x-, H_2O, and TPAOH, form. A stable clear solution containing the well-mixed moieties is then formed. The hydrolyzed HTS with hydrophilic silane head and hydrophobic tails would act as the surfactant in stabilizing the solutions. As the ethanol evaporates, the whole mixture becomes more concentrated, accompanying a self-assembly and condensation process of the moieties, and eventually a dry gel is produced. The dry gel is made of particles separated by the organic assemblies from HTS. In the subsequent hydrothermal treatment, these organic assemblies inhibit the growth of zeolitic crystals and create additional porosities by occupying a certain space between zeolitic walls. Meanwhile, TPAOH act as the direct-agent, creating the ordered micropores (MFI topology) within zeolite walls (Scheme 1).

It is interesting to observe that nanozeolites of each aggregate share the same crystalline orientation in our experimental results. To further understand the crystallization, ZSM-5-HTS samples with different crystallization times at early growth stages were investigated by TEM. Figure 8a shows that after 5 h of moisture-assisted crystallization, the material was made of spherical aggregates 0.2 to 0.5 μm in size. These spherical aggregates are made of predominantly amorphous nanoparticles (less than 5 nm). However, occasionally zeolite lattice structures can be observed in different regions in the same aggregate (Figure 8b). These lattice structures are not yet well aligned. After 24 h of reaction, further crystallization occurs. Although the particles still look amorphous in morphology (Figure 8c, and Figure 8d), a HRTEM image suggests that the aggregate is made of primary crystals, and these crystals are well-aligned and appear to be single crystalline in high resolution images (Figure 8e). These observations seem to support the mechanism that the nucleation occurs randomly in the amorphous matrix, and then the crystals grow and realign into the same orientation.

Catalytic conversion of acetone to isobutene has been found to be very sensitive to the pore structure and acidity of zeolites. Especially, the isobutene selectivity depends on the types of zeolites of various microporous structures.[42−44] Conventional ZSM-5 has been reported to be highly active for acetone conversion.

The acetone conversion to isobutene reaction was employed to study the properties of the hierarchical porous ZSM-5-HTS. For comparison, conventional ZSM-5 was also synthesized and evaluated. To exclude the effects of varying acidity, identical Si/Al ratios were used for the two catalysts studied here. The performance of the two catalysts as a function of time on stream is shown in Figure 9. It is clear that the hierarchically porous ZSM-5-HTS shows much better performance in terms of activity and isobutene selectivity. The initial conversion for ZSM-5-HTS and ZSM-5 are 69.9% and 45.7%, respectively. Initially, the isobutene formation rates were comparable for both ZSM-5 and ZSM-5-HTS. With the expected coking of the outer surface, both catalysts showed time-dependent deactivation,[43] and the

dx.doi.org/10.1021/cs200085e |*ACS Catal.* 2011, 1, 682–690

Scheme 1. Proposed Formation Mechanism for the Synthesis of Hierarchical MFI Zeolite

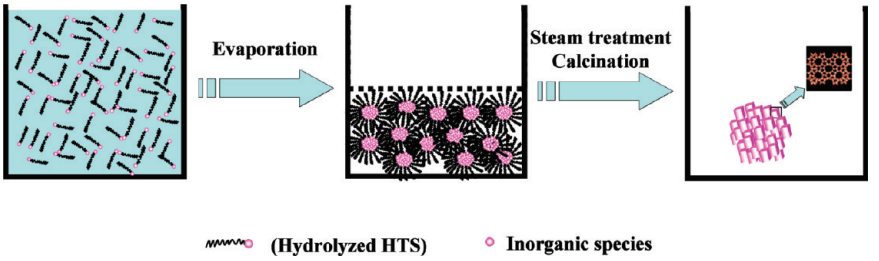

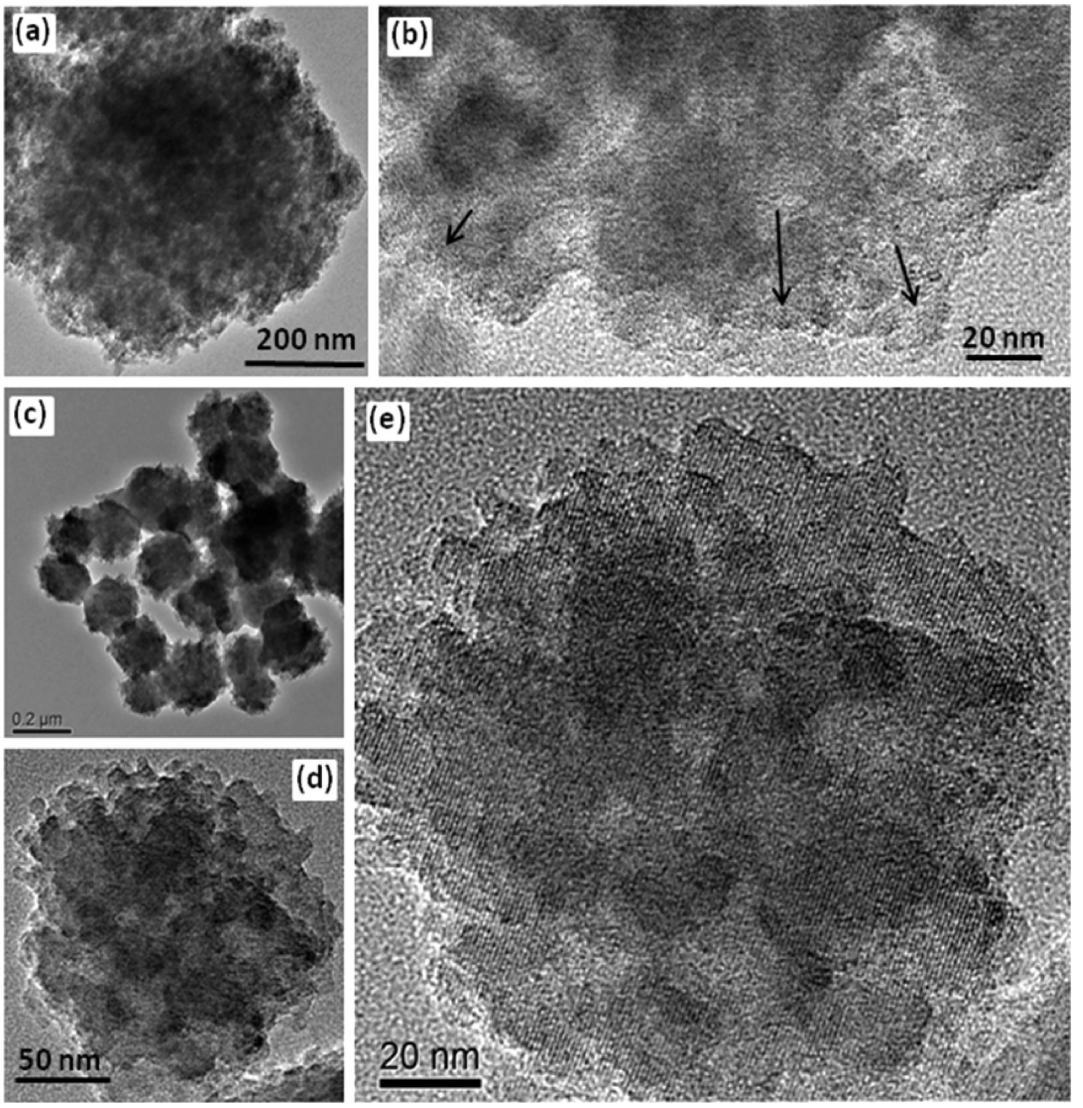

Figure 8. TEM images of ZSM-5-HTS with different crystallization time: low-magnification images of (a) 5 h and (c, d) 24 h; higher resolution images of (b) 5 h and (e) 24 h.

isobutene selectivity on both catalysts increased concomitantly. The increased isobutene selectivity suggests that the internal acidic sites became predominant and contributed to the higher selective conversion from acetone to isobutene. Noticeably, the activity on ZSM-5-HTS is always higher than that on conventional ZSM-5. At ∼ 160 min, the acetone conversion on conventional ZSM-5 drops to ∼6%, while on ZSM-5-HTS, the conversion is still >22%. After 160 min, both catalysts experienced a relatively stable period (∼4 h), during which the deactivation significantly slowed. Interestingly, the steady-state selectivity to isobutene on both catalysts is similar (∼90%), although the ZSM-5-HTS displays a higher conversion. Kinetic values suggest that the isobutene formation rate on the ZSM-5-HTS is almost four times that on the conventional ZSM-5

dx.doi.org/10.1021/cs200085e |*ACS Catal.* 2011, 1, 682–690

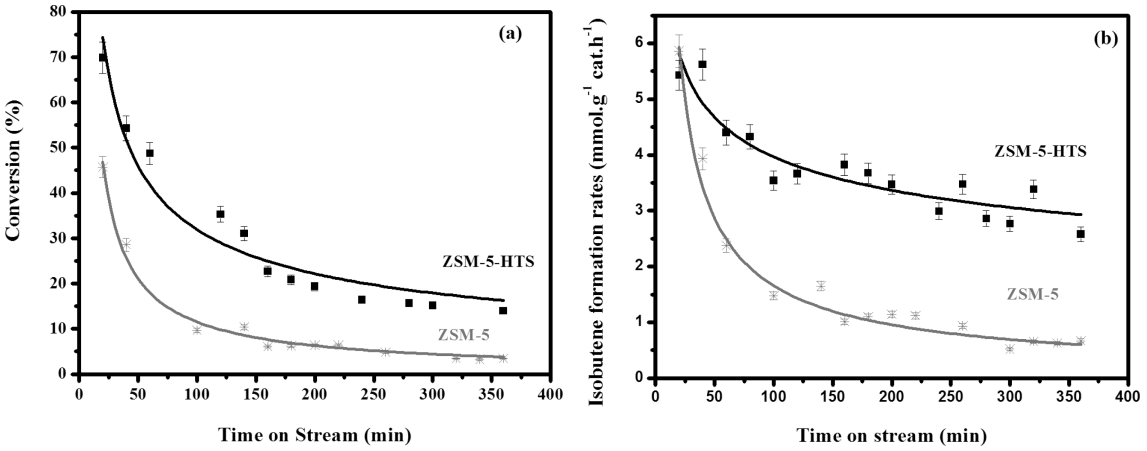

Figure 9. Catalytic production of isobutene from acetone, comparing conventional ZSM-5 (gray) and ZSM-5-HTS (black). Overall conversion and rates for isobutene formation are shown in (a) and (b), respectively.

catalysts during the steady-state acetone conversion reactions. From these results, one can conclude that the promotion of catalytic activity for ZSM-5-HTS originates from a more rapid diffusion of substrates and products through its hierarchical pores.[45] Thus, the utility of catalytically active acidic sites in zeolites is enhanced by creating additional porosity, while the selectivity for major target products is maintained.

CONCLUSIONS

A new evaporation and hydrothermal reaction method to prepare nanocrystalline and hierarchically porous zeolites has been developed. In an ethanol solution containing a structure-directing agent and siliceous and aluminum sources, hexadecyltrimethoxysilane is added to bind to zeolite particles. After ethanol evaporation, the mixture turns into a hard gel with all the nutrients for the zeolites' growth. A subsequent hydrothermal reaction crystallizes the gel to a powder form of zeolites. XRD, nitrogen physisorption, ^{27}Al MAS NMR spectra, variable-temperature HP ^{129}Xe NMR spectra, and microscopy measurements (SEM and TEM) demonstrate that hierarchically porous MFI-structured ZSM-5 crystals are produced. This material is unique and is made of nanozeolites sharing the same crystalline orientation. Porosity is formed by inhibiting the growth of zeolites with hydrophobic carbon chains during hydrothermal synthesis and defined by the intercrystal space. In the catalytic conversion of acetone to isobutene, ZSM-5-HTS shows higher catalytic activity than conventional ZSM-5 with the same Si/Al ratio by benefiting from improved mass transfer, and thus more accessible acidic sites within the hierarchical structures.

AUTHOR INFORMATION

Corresponding Author

*E-mail: jun.liu@pnl.gov.

Present Addresses

[†]UNILAB, State key laboratory of Chemical Engineering, East China University of Science and Technology, Shanghai, 200237, P. R. China.

Funding Sources

We gratefully acknowledge the U.S. Department of Energy (DOE), Office of Basic Energy Sciences, Division of Chemical Sciences, for supporting this work.

ACKNOWLEDGMENT

The TEM work described in this paper was performed at the Environmental Molecular Sciences Laboratory, a national scientific user facility sponsored by the U.S. Department of Energy (DOE) Office of Biological and Environmental Research and located at Pacific Northwest National Laboratory (PNNL). PNNL is operated for DOE by Battelle under contract number DE-AC05-76RL01830. This research is supported by the office of Basic Sciences of the U.S. Department of Energy.

REFERENCES

(1) Meier, W. M.; Olson, D. H. *Zeolites* **1992**, *12*, 1.
(2) Corma, A. *Chem. Rev.* **1997**, *97*, 2373.
(3) Tao, Y. S.; Kanoh, H.; Abrams, L.; Kaneko, K. *Chem. Rev.* **2006**, *106*, 896.
(4) Perez-Ramirez, J.; Christensen, C. H.; Egeblad, K.; Groen, J. C. *Chem. Soc. Rev.* **2008**, *37*, 2530.
(5) Su, L. L.; Liu, L.; Zhuang, J. Q.; Wang, H. X.; Li, Y. G.; Shen, W. J.; Xu, Y. D.; Bao, X. H. *Catal. Lett.* **2003**, *91*, 155.
(6) Schmidt, I.; Madsen, C.; Jacobsen, C. J. H. *Inorg. Chem.* **2000**, *39*, 2279.
(7) Wang, H. T.; Holmberg, B. A.; Yan, Y. S. *J. Am. Chem. Soc.* **2003**, *125*, 9928.
(8) Vuong, G. T.; Do, T. O. *J. Am. Chem. Soc.* **2007**, *129*, 3810.
(9) Serrano, D. P.; Aguado, J.; Escola, J. M.; Rodriguez, J. M.; Peral, A. *Chem. Mater.* **2006**, *18*, 2462.
(10) Xin, H.; Koekkoek, A.; Yang, Q.; van Santen, R.; Li, C.; Hensen, E. J. M. *Chem. Commun.* **2009**, 7590.
(11) Srivastava, R.; Iwasa, N.; Fujita, S.; Arai, M. *Chem.—Eur. J.* **2008**, *31*, 9507.
(12) Serrano, R.; Aguado, J.; Morales, G.; Rodriguez, J. M.; Peral, A.; Thommes, M.; Epping, J. D.; Chmelka, B. F. *Chem. Mater.* **2009**, *21*, 641.
(13) Petushkov, A.; Yoon, S.; Larsen, S. C. *Microporous Mesoporous Mater.* **2011**, *137*, 92.
(14) Chen, Z. W.; Li, S.; Yan, Y. S. *Chem. Mater.* **2005**, *17*, 2262.
(15) Jacobsen, C. J. H.; Madsen, C.; Houzvicka, J.; Schmidt, I.; Carlsson, A. *J. Am. Chem. Soc.* **2000**, *122*, 7116.
(16) Christensen, C. H.; Johannsen, K.; Schmidt, I. *J. Am. Chem. Soc.* **2003**, *125*, 13370.
(17) Schmidt, I.; Krogh, A.; Wienberg, K.; Carlsson, A.; Brorson, M.; Jacobsen, C. J. H. *Chem. Commun.* **2000**, 2157.
(18) Zhu, K. K.; Hu, J.; She, X.; Liu, J.; Nie, Z.; Wang, Y.; Peden, C.; Kwak, J. *J. Am. Chem. Soc.* **2009**, *131*, 9715.
(19) Tao, Y. S.; Kanoh, H.; Kaneko, K. *J. Am. Chem. Soc.* **2003**, *125*, 6044.

(20) Xiao, F. S.; Wang, L. F.; Yin, C. Y.; Lin, K. F.; Di, Y.; Li, J. X.; Xu, R. R.; Su, D. S.; Schlogl, R.; Yokoi, T.; Tatsumi, T. *Angew. Chem., Int. Ed.* **2006**, *45*, 3090.
(21) Zhu, K.; Egeblad, K.; Christensen, C. H. *Eur. J. Inorg. Chem.* **2007**, 3955.
(22) Kustova, M.; Egeblad, K.; Zhu, K.; Christensen, C. H. *Chem. Mater.* **2007**, *19*, 2915.
(23) Zhu, H. B.; Liu, Z. C.; Kong, D. J.; Wang, Y. D.; Xie, Z. K. *J. Phys. Chem. C* **2008**, *112*, 17257.
(24) Choi, M.; Cho, H. S.; Srivastava, R.; Venkatesan, C.; Choi, D. H.; Ryoo, R. *Nat. Mater.* **2006**, *5*, 718.
(25) Wang, H.; Pinnavaia, T. J. *Angew. Chem., Int. Ed.* **2006**, *45*, 7603.
(26) Yang, P. D.; Zhao, D. Y.; Margolese, D. I.; Chmelka, B. F.; Stucky, G. D. *Nature* **1998**, *396*, 152.
(27) Xue, C. F.; Tu, B.; Zhao, D. Y. *Adv. Funct. Mater.* **2008**, *18*, 3914.
(28) Meng, Y.; Gu, D.; Zhang, F. Q.; Shi, Y. F.; Yang, H. F.; Li, Z.; Yu, C. Z.; Tu, B.; Zhao, D. Y. *Angew. Chem., Int. Ed.* **2005**, *44*, 7053.
(29) Shimojima, A. *J. Ceram. Soc. Jpn.* **2008**, *116*, 278.
(30) Fujimoto, Y.; Shimojima, A.; Kuroda, K. *J. Mater. Chem.* **2006**, *16*, 986.
(31) Shimojima, A.; Kuroda, K. *Angew. Chem., Int. Ed.* **2003**, *42*, 4057.
(32) Shimojima, A.; Liu, Z.; Ohsuna, T.; Terasaki, O.; Kuroda, K. *J. Am. Chem. Soc.* **2005**, *127*, 14108.
(33) Lu, Y. F.; Fan, H. Y.; Stump, A.; Ward, T. L.; Rieker, T.; Brinker, C. J. *Nature* **1999**, *398*, 223.
(34) Brinker, C. J.; Lu, Y. F.; Sellinger, A.; Fan, H. Y. *Adv. Mater.* **1999**, *11*, 579.
(35) Mueller, U.; Unger, K. K. *Zeolites* **1988**, *8*, 154.
(36) Wang, L. Q.; Karkamkar, A.; Autrey, T.; Exarhos, G. J. *J. Phys. Chem. C* **2009**, *113*, 6485.
(37) Wu, E. L.; Lawton, S. L.; Olson, D. H.; Rohrman, A. C.; Kokotailo, G. T. *J. Phys. Chem.* **1979**, *83*, 2777.
(38) Groen, J. C.; Peffer, L. A. A.; Perez-Ramirez, J. *Microporous Mesoporous Mater.* **2003**, *60*, 1.
(39) Buhl, J. C.; Lons, J. *J. Alloys Compd.* **1996**, *235*, 41.
(40) Liu, Y.; Zhang, W. P.; Liu, Z. C.; Xu, S. T.; Wang, Y. D.; Xie, Z. K.; Han, X. W.; Bao, X. H. *J. Phys. Chem. C* **2008**, *112*, 15375.
(41) Dong, W. Y.; Sun, Y. J.; Lee, C. W.; Hua, W. M.; Lu, X. C.; Shi, Y. F.; Zhang, S. C.; Chen, J. M.; Zhao, D. Y. *J. Am. Chem. Soc.* **2007**, *129*, 13894.
(42) Chang, C. D.; Silvestri, A. J. *J. Catal.* **1977**, *47*, 249.
(43) Hutchings, G. J.; Johnston, P.; Lee, D. F.; Williams, C. D. *Catal. Lett.* **1993**, *21*, 49.
(44) Nedomova, K.; Beran, S.; Jiru, P. *React. Kinet. Catal. Lett.* **1986**, *32*, 353.
(45) Christensen, C. H.; Johannsen, K.; Törnqvist, E.; Schmidt, I.; Topsøe, H.; Christensen, C. H. *Catal. Today* **2007**, *128*, 117.